

Seismic fragility assessment of bridge piers incorporating high-strength steel reinforcement and concrete

S. Aldabagh, S. Khan & M.S. Alam
University of British Columbia, Kelowna, Canada

ABSTRACT: Design codes in the United States and Canada limit the use of high-strength steel (HSS) and high-strength concrete (HSC) in bridge components that are capacity-protected during a seismic event. Although HSS and HSC have higher tensile and compressive strength, respectively, their lower inelastic strain capacity imposes for such restrictions. To assess the seismic performance of HSS and HSC, the pier of an existing bridge is redesigned using concrete compressive strength of 50 and 80 MPa, and reinforcement yield strength of 420, 690, and 830 MPa. Static pushover and nonlinear dynamic time-history analyses were performed to generate force-deformation and seismic fragility curves. Bridge piers incorporating HSS and HSC attained the maximum load capacity yet were the least ductile. They are less seismically vulnerable than those incorporating conventional materials at minimal and repairable damage states, but not at extensive and probable replacement damage states.

1 INTRODUCTION

High-strength steel (HSS) reinforcement conforming to the requirements of ASTM A1035 (ASTM 2019) is being produced in the United States and Canada in two grades, namely, Grade 690 and Grade 830. HSS lacks a distinct yield plateau and therefore, establishing its yield strength (f_y) requires using one of the following methods: (1) the 0.35% extension under load (EUL) method; (2) the 0.5% EUL method; and (3) the 0.2% offset method (most commonly used in practice). In the 0.2% offset method, the yield strength is established at the intersection of a line whose slope and starting point equal to the modulus of elasticity of steel and 0.2% strain, respectively, with the engineering stress-strain curve. Grade 690 and 830 exhibit a minimum yield strength of 690 and 830 MPa, respectively, based on the 0.2% offset method. The modulus of elasticity of the two grades is 200 GPa, and the tensile strength for Grade 690 and 830 is 1070 and 1100 MPa, respectively (WJE 2008). The stress-strain curve of the ASTM A1035 Grade 690 reinforcing bar used in this study is shown in Figure 1. The use of the aforementioned methods to establish the f_y of ASTM A1035 Grade 690 reinforcing bar is illustrated in Figure 1.

Since HSS exhibits considerably higher strength than conventional Grade 420 steel, it allows for a substantial reduction in the required area of reinforcement resulting in improved placement and workability of concrete, especially in heavily reinforced sections which are often part of the seismic force-resisting systems. HSS often balances the increase in material cost by reducing the labor cost, which is a function of the material weight (Thomas et al. 2013). In addition, several researchers have reported that HSS is noticeably more corrosion-resistant than conventional steel (Seliem 2007; Darwin et al. 2009; Ji et al. 2005; Clemena and Virmani 2004). The better performance of HSS in corrosion resistance, compared to conventional steel, is primarily due to the higher chromium content. There have been several successful attempts to introduce HSS in bridge decks. Seliem (2007) reported that the use of HSS in concrete bridge decks reduces the amount of required longitudinal reinforcement by 33% without compromising the load-carrying capacity or altering the serviceability behavior of the bridge deck. In addition, according to Pedro et al. (2018), the use of HSS in steel-concrete bridge decks allows for a reduction of 25 to 30% in the steel weight. Saleem et al. (2011) utilized HSS and ultrahigh-performance concrete to develop an innovative lightweight bridge deck system to replace the open-grid steel decks from moveable bridges. It is clear from the previous examples that HSS can be a promising alternative to conventional steel in bridge decks; however, extending its application to bridge

piers requires further attention due to two main reasons. First, bridge piers are usually susceptible to damage during a seismic event, i.e. the location where inelastic deformation is expected to occur. Second, the substantial difference in material properties between conventional steel and HSS may lead to noticeable differences in seismic response (Aldabagh and Alam 2020). While designing reinforced concrete (RC) structural elements against seismic forces, several material properties of reinforcing steel must be carefully examined. These include: (1) minimum yield strength; (2) tensile strength; (3) uniform elongation and total elongation; (4) ratio of tensile strength to yield strength. For conventional steel, ASTM (2016) requires that the tensile strength shall not be less than 1.25 times the actual yield strength. This is an important limit since the yield ratio controls the length of yield region along the axis of the members, and thus contributes directly to the plastic rotation capacity. In ASTM A1035 reinforcement, the yield ratio is normally found to exceed 1.25 if the yield strength is established based on the 0.2% offset method (WJE 2008). However, the elongation, which is another important measure of ductility, of ASTM A1035 reinforcement is lower than that of ASTM A706 reinforcement. As a result, due to the uncertainty associated with the ductility of members containing ASTM A1035 Grade 690 and Grade 830 reinforcement, the AASHTO Guide Specifications for LRFD Seismic Bridge Design (AASHTO 2017) limits the use of such reinforcement to members which are expected to remain elastic, i.e. not part of the seismic-force resisting system. The Canadian Highway Bridge Design Code (CHBDC) (CSA S6 2019), on the other hand, does not permit the use of ASTM A1035 reinforcing bars in both non-seismic and seismic applications.

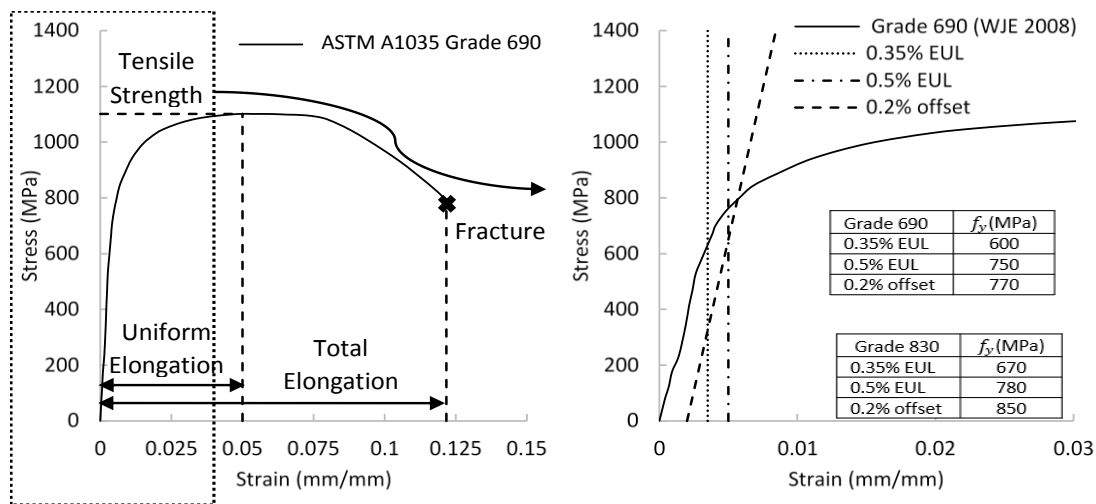


Figure 1. Stress-strain response of ASTM A1035 Grade 690 reinforcing bar (WJE 2008).

Several researchers have evaluated the performance of concrete columns reinforced with HSS under quasi-static reversed cyclic loading (Restrepo et al. 2006; Rautenberg et al. 2013; Barbosa et al. 2016; Li et al. 2018; and Lim et al. 2017). Concrete columns reinforced with HSS are more flexible than those reinforced with a larger amount of conventional steel. Rautenberg et al. (2013) reported that columns reinforced with HSS reinforcement were characterized by a high drift ratio at yield (1.4-1.7%), which was up to 90% higher than that measured in specimens reinforced with conventional steel. Concrete columns reinforced with HSS were characterized with less ductile response than those reinforced with conventional steel, and hence dissipated less energy (Rautenberg et al. 2013). However, Rautenberg et al. (2013) reported, based on numerical analysis that multi-story moment reinforced concrete frame buildings built with columns reinforced with HSS experience less larger drifts than those built with columns reinforced with conventional steel. Concrete bridge columns reinforced with HSS can resist up to 4% of drift ratio demand before failure (Restrepo et al. 2006). Concrete columns reinforced with HSS are characterized with moment resistance, maximum top lateral displacement, and curvature ductility comparable to that of columns reinforced with conventional steel (Barbosa et al. 2016).

In addition to HSS, high-strength concrete (HSC) is another high-performance material (HPM) that has been gaining popularity for many years due to its numerous advantages over normal strength concrete (NSC). Since HSC exhibits concrete compressive strength (f_c) higher than NSC, utilizing it in buildings leads to a considerable reduction in the column sizes. This is mostly beneficial in high-rise buildings where the columns in lower stories are larger in size. Besides, HSC has other advantages related to lateral stiffness and axial shortening (Colaco et al. 1985). However, HSC is more brittle than NSC, and therefore, requires additional attention when extending current design code requirements to the design and detailing of HSC columns

located in seismically active regions. According to Cusson et al. (1994) and Razvi et al. (1994), increasing the amount of transverse reinforcement is necessary to maintain a constant level of ductility for columns subjected to the same level of axial load. Studies have shown that HSC columns, whose transverse reinforcement is designed as per the ACI confinement requirements, exhibit adequate ductility when subjected to axial loads below 20% of column axial load capacity (Légeron et al. 2000; Azizinamini et al. 1994; and Bayrak et al. 1998). In addition, Paultre et al. (2009) demonstrated that HSC circular columns designed according to the CSA A23.3 requirements are characterized by ductile performance regardless of the yield strength of transverse reinforcement and axial load ratio. HSS and HSC have the potential of replacing current conventional materials in members resisting seismic forces if the design code requirements are met and proper reinforcement detailing is provided (Aldabagh and Alam 2020). However, before introducing design guides related to the use of HPMs, it is crucial to evaluate the seismic performance of structures incorporating such materials. The seismic performance of concrete buildings utilizing HPMs such as HSS and HSC have been evaluated numerically by Billah and Alam (2013) and Konstantinidis and Kappos (2003). It was concluded that introducing such materials improved the seismic performance of the buildings by reducing the probability of failure when compared to normal strength materials. However, there is a lack of research works evaluating the seismic vulnerability of bridge piers incorporating HPMs. Therefore, this study aims to perform a fragility-based seismic vulnerability assessment of a bridge pier incorporating different combinations of HSC and HSS under near-fault ground motions. Fragility curves are often effective in expressing the seismic vulnerability since they identify the probability of a structure sustaining a particular level of damage when subjected to certain ground acceleration. In this paper, the design of a bridge pier in Vancouver, British Columbia is initially verified using normal strength materials, i.e. the actual materials used in the construction of the bridge. Then, based on the force-based seismic design procedure prescribed in the CHBDC (CSA S6 2019), the bridge pier is redesigned using different combinations of HPMs. The seismic performance of the proposed bridge pier sections is assessed using nonlinear static-pushover and dynamic time history analyses. The findings of this research are expected to reduce the concerns over the seismic performance of bridge piers reinforced with HSS and cast with HSC. In addition, design recommendations for the design of single-column bridge piers are proposed based on the results of the fragility-based seismic assessment. Hence, this research should help relax current restrictions related to the use of HPMs found in the bridge design codes (such as CHBDC and AASHTO), and consequently, allow bridge engineers to make efficient use of their potential benefits.

2 GEOMETRY AND DESIGN OF PROTOTYPE BRIDGE

A two-span continuous concrete girder bridge located in Vancouver, British Columbia, Canada was selected for this study. The bridge is representative of the inventory for this particular bridge type of Western Canada. The configuration of the bridge is illustrated in Figure 2. The bridge has two spans, which are 19.5 and 22 m long for a total length of 41.5 m. The width of the bridge deck is 10 m, which is composed of a 235 mm thick composite reinforced concrete deck supported by 3 MOTI Type IV precast pretensioned I-girders (D202 2006). The deck has a full integral connection at both abutment and pier locations, making the bridge a continuous bridge. The bridge bent consists of a single circular column 1.22 m in diameter and 8.8 m in height. The total superstructure self-weight from the two half spans carried by the pier is 2450 kN. The material properties used in the original design were $f_y = 420$ MPa and $f'_c = 35$ MPa. In the original design, the column reinforcement consists of 22-35M longitudinal reinforcement and a 20M spiral with a pitch of 75 mm in the plastic hinge region.

In this study, section diameter of 914 mm, reinforcement with f_y of 420, 690, and 830 MPa, and concrete with f'_c of 50 and 80 MPa are considered, resulting in a total of 6 different sections. The middle pier of the considered bridge was redesigned using these proposed sections. The force-based design procedure was initially validated by designing the bridge pier using its original section and material properties described earlier. A Response modification factor, R , of 4 and an importance factor, I_E , of 1.5 were assigned in the design of all sections, as prescribed in the CHBDC (CSA S6 2019). A thorough review of bent column SLS stress and cracking requirements for non-seismic loads per CHBDC (CSA S6 2019) is beyond the scope of this manuscript. However, the seismic performance of the bridge pier at different hazard levels was compared against the performance criteria of the CHBDC (CSA S6 2019) as part of the performance-based design framework. The sections were labeled to indicate section diameter, reinforcement strength, and concrete strength—for example, 914-420-50 refers to bridge pier section with 914 mm diameter, 420 MPa reinforcement yield strength, and 50 MPa concrete compressive strength. Table 1 lists these sections, along with the output of the force-based design (design base shear (V), longitudinal reinforcement ratio (ρ_l), and spiral transverse reinforcement ratio (ρ_s)). Axial load ratio, which is defined as the ratio of the applied load

(P), to the gross area of section (A_g) multiplied by f'_c , ranged between 4.8% and 7.7% due to the change in f'_c . The axial load ratios are close to 5 % which is the approximate average design axial load ratio of bridge piers in seismic regions (Sritharan et al. 2007). Besides, the aspect ratio, which is the ratio of the height to diameter of the column, was more than 4 for all the sections, ensuring flexure-controlled failure.

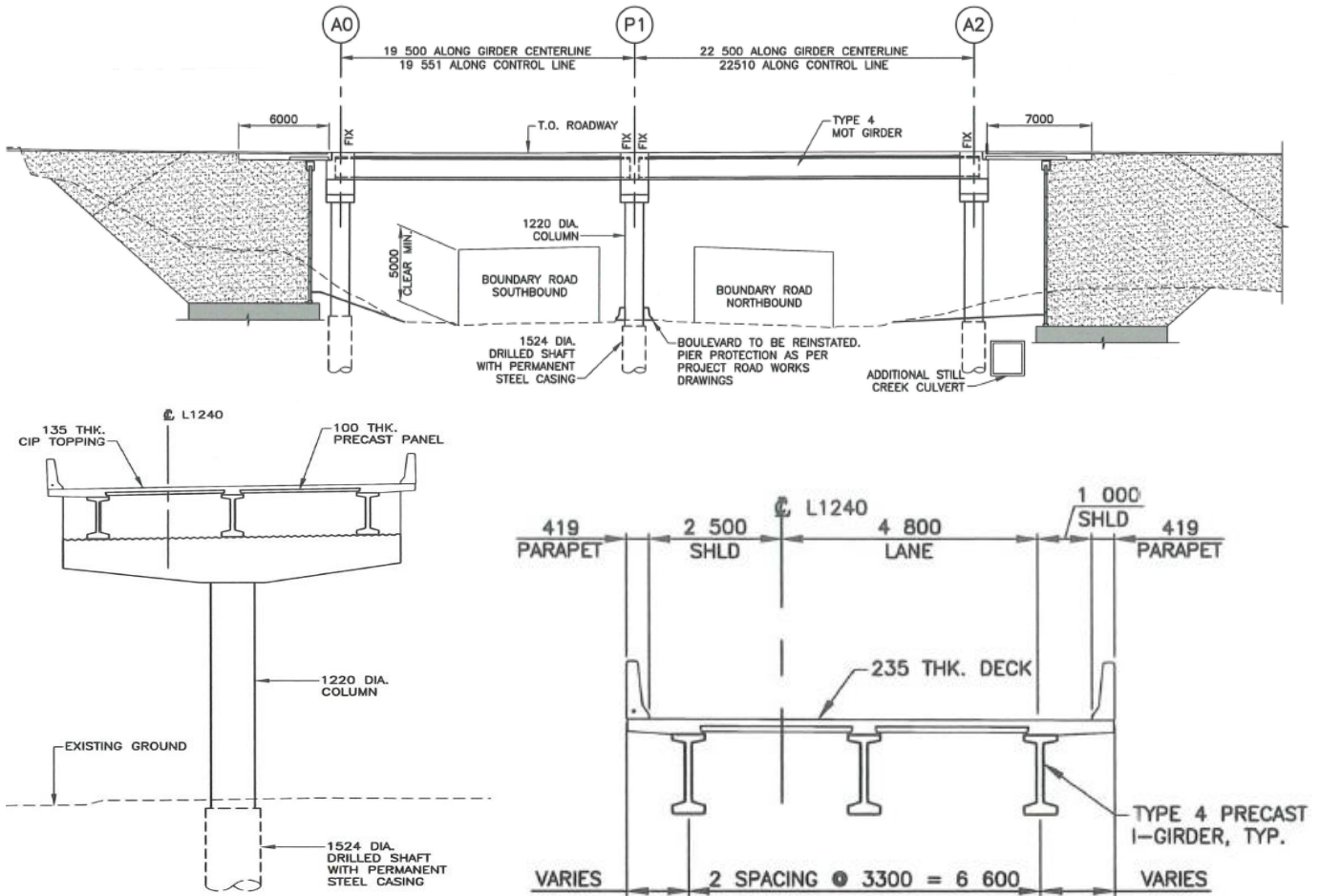


Figure 2. Selected bridge configuration (dimensions are in mm) (reproduced with permission from the project team).

Table 1. Summary of the force-based design results.

Section	ϕ (mm)	f_y (MPa)	f'_c (MPa)	$P/A_g f'_c$ (%)	V (kN)	ρ_l (%)	ρ_s (%)
1220-420-35*	1220	420	35	6.0	324	1.9	1.5
914-420-50	914	420	50	7.7	238	3.7	1.5
914-420-80	914	420	80	4.8	238	3.4	2.4
914-690-50	914	690	50	7.7	210	1.8	0.9
914-690-80	914	690	80	4.8	219	1.7	1.4
914-830-50	914	830	50	7.7	200	1.5	0.75
914-830-80	914	830	80	4.8	210	1.4	1.2

* Original section of the bridge pier.

3 FINITE ELEMENT MODELING AND MODEL VERIFICATION

SeismoStruct (Seismosoft 2018), a finite-element package featuring fiber-based modeling for structural analysis, is used in this study to perform the static pushover and nonlinear dynamic time history analysis. The bridge pier is modeled using inelastic displacement-based element (DBE), in which constant axial deformation and linear curvature distribution are enforced along the element length to approximate the response. Therefore, when utilizing such elements, the member is often subdivided into members of smaller lengths to achieve higher accuracy, particularly in the plastic hinge region. Figure 3 shows the finite element model of the bridge, along with the discretized section. Rayleigh damping with initial stiffness was used to model the energy dissipation in the bridge pier. To simulate bar-slip rotations, an elastic rotational spring was used at the column end, as shown in Figure 3. The rotational stiffness of the bond-slip springs (K_{SE}) is given by the following equation:

$$K_{SE} = \frac{2M_y}{\phi_y l_{sp}} \quad (1)$$

Where, M_y is the yield moment of the section, ϕ_y is the corresponding yield curvature, and l_{sp} is effective strain penetration depth at bar yield. l_{sp} is defined as follows (Elwood and Eberhard 2009):

$$l_{sp} = \frac{1}{3.2} \frac{f_y}{\sqrt{f'_c}} d_b \quad (2)$$

Where d_b is the diameter of the longitudinal rebar. Menegotto-Pinto steel model (Menegotto and Pinto 1973) was used to model the material properties of the reinforcing steel. In the case of HSS, the model parameters were modified to produce a similar stress-strain relationship to that of HSS. Several researchers have successfully utilized the Menegotto-Pinto steel model to evaluate the seismic behavior of structures incorporating HSS reinforcement (Billah and Alam 2013; Laughery 2016). Nevertheless, the accuracy of the models utilized in this paper was validated using experimental results of concrete columns reinforced with conventional steel and HSS and tested under cyclic loading. Normal-strength concrete material properties were incorporated into the model using Mander et al. (1988) nonlinear concrete model, while the HSC properties were incorporated into the model using Kappos and Konstantinidis (1999). The 2450 kN self-weight of the superstructure is applied on top of the column, as shown in Figure 3.

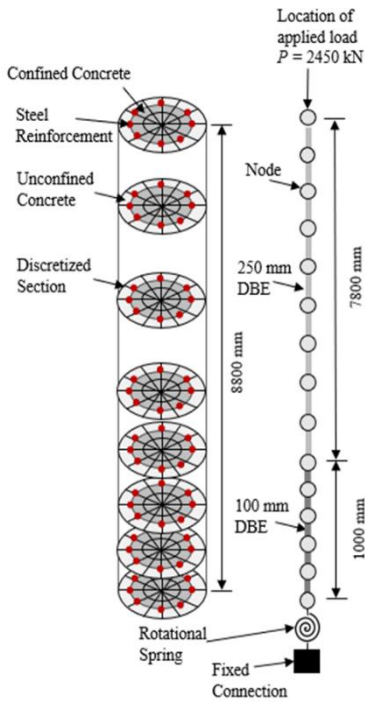


Figure 3. Finite element modeling of the bridge pier.

The numerical models described above are validated with experimental results of concrete columns reinforced with conventional steel (Moyer and Kowalsky 2003), and HSS (Restrepo et al. 2006). The reader may refer to the corresponding research work for additional details on the experimental tests. Figure 4 shows a comparison between the experimental and numerical responses for columns reinforced with conventional steel and HSS. It is observed that for the two specimens, the maximum shear force and displacement are predicted within 10% error and strength decay, stiffness degradation, and energy dissipation are accurately reflected in the models.

4 FRAGILITY FUNCTION METHODOLOGY

Fragility curves are critical in the seismic risk assessment of bridges since they describe the level of damage to the bridge components when subjected to different levels of ground shaking. Direct comparison of vulnerability functions or so-called fragility curves of different bridge design alternatives is an effective approach in selecting the optimal bridge design. However, constructing these curves might not be practical (for certain cases) due to the amount of time and effort required to develop them, as will be illustrated in this

section. A fragility function represents the conditional probability of meeting or exceeding a given damage state (or performance) for a given ground motion intensity measure. This conditional probability function can be expressed as follows:

$$Fragility = P[LS|IM = y] \quad (3)$$

Where, LS is the limit state (or performance) or level of damage to the bridge component; IM is the ground motion intensity measure; and y is the realized condition of the chosen ground motion intensity measure. The realization of the ground motion intensity measure is normally achieved by expressing y in terms of peak ground acceleration or spectral acceleration at the fundamental period.

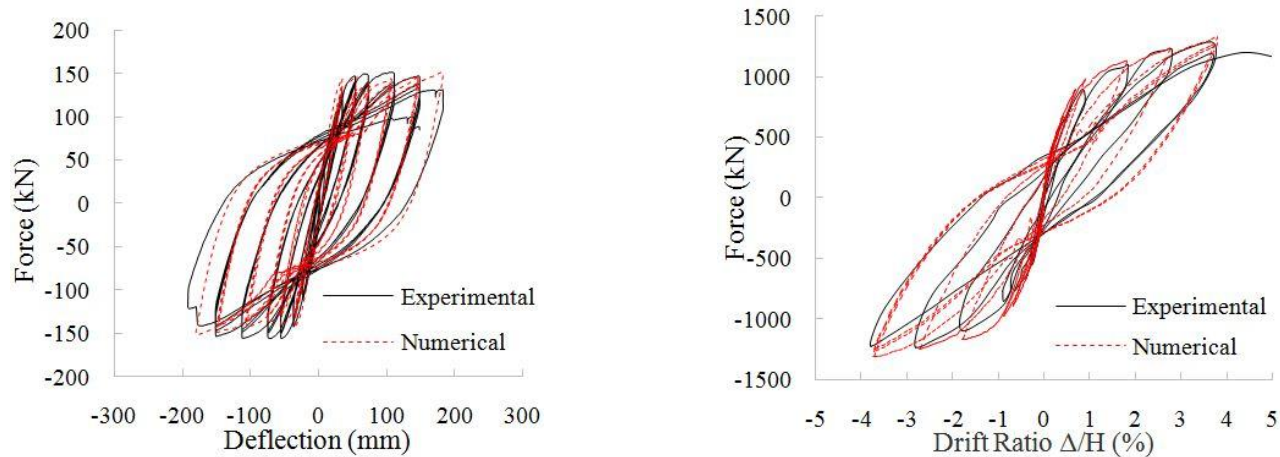


Figure 4. Comparison of experimental and numerical responses of column reinforced with (a) conventional steel (Moyer and Kowalsky 2003), and (b) ASTM A1035 Grade 690 steel (Restrepo et al. 2006).

5 RESULTS

5.1 Static Push-Over Analysis

Static pushover analysis has been performed to assess the performance of the bridge pier sections when subjected to constant gravity load and monotonically increasing lateral displacement pattern of constant shape. Table 2 provides a summary of the main characteristics including initial stiffness (K_i), maximum load (F_m), ultimate load (F_u), drift ratio at yield (Δ_y/H), drift ratio at ultimate (Δ_u/H), displacement ductility (μ_Δ), curvature at yield (ϕ_y), curvature at ultimate (ϕ_u), curvature ductility (μ_ϕ), and ultimate to displacement demand ratio ($\Delta_u/\Delta_{2\%}$) extracted from the pushover curve for each section. The drift ratio at yield (Δ_y/H) and ultimate (Δ_u/H) are defined as the ratio of lateral top displacement at yield (Δ_y) and ultimate (Δ_u), respectively, to the height of the pier (H). The ultimate displacement to displacement demand ratio ($\Delta_u/\Delta_{2\%}$) is the ratio of Δ_u to the displacement demand at hazard level of 2% probability of exceedance in 50 years. F_m is the maximum recorded load, whereas F_u is the load established at 10% drop in F_m . In the pushover analysis, bridge piers were subjected to a target drift demand of 9% to determine its ultimate capacity. The ultimate lateral load capacity is taken as the point corresponding to a 10% reduction in strength compared to the peak load as per Elnashai and Sarno (2008). A larger target drift was chosen to ensure that all bridge piers experience a 10% reduction in strength beyond its peak load. The yield drift is defined as the drift corresponding to the yield point of an equivalent system with elastic-perfectly plastic response and the same energy dissipation as the original system (Park 1988). μ_Δ and μ_ϕ are defined as the ratio of displacement and curvature at ultimate, respectively, to the corresponding values at yield. Sections reinforced with steel having higher yield strength and cast with concrete having higher concrete compressive strength attained higher F_m and F_u when compared to the reference section, i.e. section with $f_y = 420$ MPa and $f'_c = 50$ MPa. Sections reinforced with Grade 690 and 830 steel were characterized with higher drift ratio at yield but lower drift ratio at ultimate when compared to sections reinforced with Grade 420 steel. The higher drift ratio at yield in such sections is attributed to the higher strain levels required for Grade 690 and 830 steel to yield when compared to Grade 420 steel. Sections incorporating HSS reinforcement generally are characterized by lower displacement and curvature ductility when compared to the sections reinforced with conventional steel. This is primarily due to the higher load required to yield Grade 690 and 830 steel and the lower ultimate rupture strain when compared to Grade 420 steel. The displacement ductility of sections with $f'_c = 80$ MPa decreased by 2%-22% when compared to that of sections with $f'_c = 50$ MPa.

Table 2. Summary of the static pushover analysis results.

Section	K_i (kN/mm)	F_m (kN)	F_u (kN)	Δ_y/H (%)	Δ_u/H (%)	μ_Δ	Φ_y ($\times 10^{-6}$ 1/mm)	Φ_u ($\times 10^{-6}$ 1/mm)	μ_Φ	$\Delta_u/\Delta_{2\%}$ (%)
914-420-50	5.5	355	320	1.2	5.1	4.1	4.3	70.6	16.3	1.7
914-420-80	7.2	380	342	1.2	4.0	3.4	4.2	50.5	12.0	1.4
914-690-50	4.7	353	319	1.9	7.0	3.6	7.0	69.4	9.9	1.7
914-690-80	6.6	365	329	1.8	6.0	3.3	6.7	52.4	7.8	1.5
914-830-50	4.7	317	286	2.2	7.0	3.2	8.4	64.7	7.7	1.6
914-830-80	6.5	341	307	2.2	5.4	2.5	7.8	52.4	6.7	1.3

5.2 Fragility Curves

One of the simplest ways of comparing the seismic performance of the sections is to identify the relative change in the median value of the fragility estimate. The percent change in the median values relative to the reference sections is listed in Table 3. In this study, the reference section was 914-420-50. A positive percent change in the median indicates a shift in the fragility curve to the right, i.e. less vulnerable section, while a negative percent change in the median value indicates a shift to the left, i.e. more vulnerable section. For each damage state, the section with the largest positive percent difference in the median is the least vulnerable.

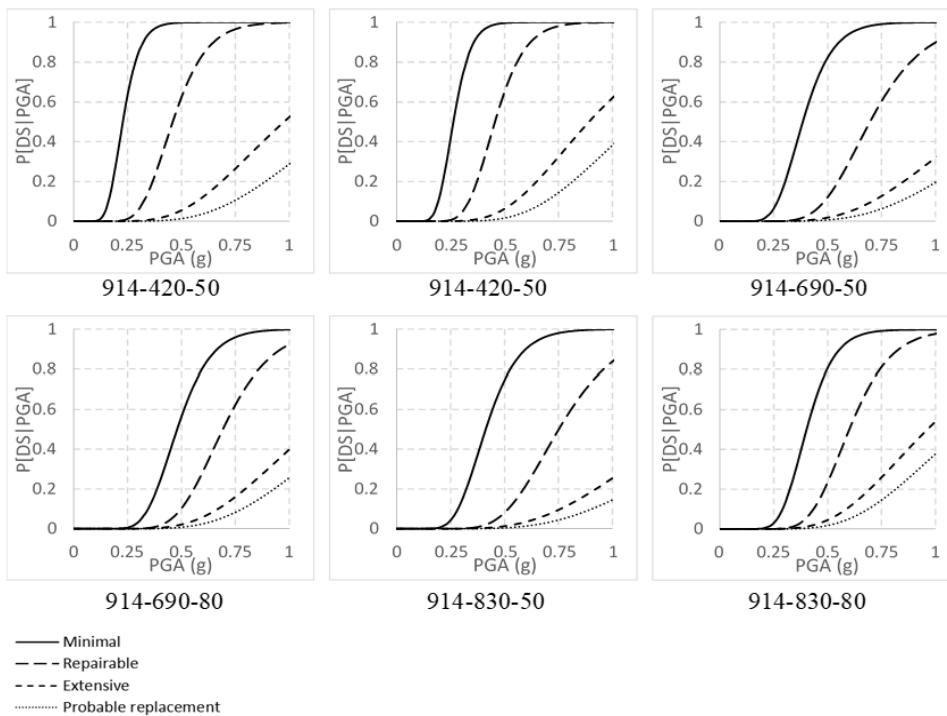


Figure 5. Fragility curves of all sections.

In Table 3, the section with the largest median improvement for each damage state is presented in boldface type. Section 914-690-80 was the least vulnerable for the minimal damage state, while section 914-830-50 was the least vulnerable for repairable, extensive, and probable replacement damage states. For minimal and repairable damage states, sections incorporating HSS and HSC are always less vulnerable than the reference section whereas, for extensive and probable replacement damages states, this is not true since some sections are characterized with negative percent change in the median value indicating a more vulnerable section when compared to the reference section. However, it was interesting to observe that all the sections having a negative percent change in the median value, the percent change is relatively small and does not exceed 10%. This appears to be similar to the findings of Billah and Alam (2013) who evaluated the seismic performance of concrete columns in buildings incorporating HPMs. Based on the previous findings of the fragility assessment, designing bridge piers reinforced with HSS using a response modification factor of 4 yielded sections exhibiting better seismic performance for the minimal and repairable damages states, and comparable seismic performance for extensive and probable replacement damage states when compared to the performance of bridge piers reinforced with conventional steel. Besides, all of the sections incorporating HSS and HSC met the criteria of the performance-based design prescribed in the CHBDC (CSA S6 2019).

However, in certain sections, displacement ductility capacity was less than 4, making them unsuitable for a force reduction factor of 4. For this reason, further research work is warranted before incorporating the response modification factor into the CHBDC applicable to bridge piers incorporating HPMs to examine a wider range of column diameters, concrete compressive strengths, ground motions, and possibly other bridge bent configurations. The fragility curves for all sections generated based on the analytical procedure outlined in an earlier section of this paper are shown in Figure 5.

Table 3. Percent difference in fragility medians PGA for all sections relative to the reference sections.

Section	% Difference in median PGA from reference section			
	Minimal	Repairable	Extensive	Probable Replacement
914-420-50	-	-	-	-
914-420-80	+14	-0	-10	+3
914-690-50	+66	+51	+23	+36
914-690-80	+109	+51	+10	+19
914-830-50	+79	+64	+34	+47
914-830-80	+74	+31	-4	+3

6 SUMMARY AND CONCLUSIONS

A coordinated analytical and numerical research program is conducted to evaluate the seismic performance of an existing bridge in Vancouver, British Columbia when different combinations of HSS and HSC are incorporated into its middle pier. The following conclusions are drawn:

- Bridge piers designed based on the force-based design approach and reinforced with HSS are characterized with less amount of longitudinal and transverse reinforcement steel when compared to those reinforced with conventional steel.
- Based on the static pushover analysis, columns containing HSS and HSC exhibit higher load capacity, yet less ductility capacity, when compared to columns with $f_y = 420$ MPa and $f'_c = 50$ MPa. Extending the applicability of performance criteria for bridge piers reinforced with conventional steel to bridge piers reinforced with HSS yield reasonable results when carrying performance-based design. However, future research work is required to develop performance criteria specifically applicable to columns reinforced with HSS.
- Bridge piers incorporating HSS and HSC are less seismically vulnerable than those incorporating normal-strength steel and concrete for minimal and repairable damage states but not extensive and probable replacement damage states.

ACKNOWLEDGEMENTS

The financial contributions of McElhanney, Vancouver, and Mitacs through Accelerate Grant are gratefully acknowledged. The drawings were provided by the British Columbia (BC) Ministry of Transportation and Infrastructure officials. Their help is also gratefully acknowledged.

REFERENCES

- AASHTO.2017. LRFD bridge design specifications. American Association of State Highway Officials, Washington, D.C.
- Aldabagh, S., and Alam, M. S. High-strength steel reinforcement (ASTM A1035/A1035M Grade 690): state-of-the-art review. *J. Struct. Eng.*, 146(8), 03120003.
- ASTM A1035 / A1035M-19. 2019. Standard specification for deformed and plain, low-carbon, chromium, steel bars for concrete reinforcement. ASTM International, West Conshohocken, PA.
- ASTM A706 / A706M-16. 2016. Standard Specification for Deformed and Plain Low-Alloy Steel Bars for Concrete Reinforcement, ASTM International, West Conshohocken, PA.
- Azizinamini, A.; Baum Kuska, S. S.; Brungardt, P.; and Hatfield, E. 1994. Seismic behavior of square high-strength concrete columns. (1994). *ACI Structural Journal*, 91(3), 336-345.
- Barbosa, A. R., Link, T., and Trejo, D. 2016. Seismic performance of high-strength steel RC bridge columns. *Journal of Bridge Engineering*, 21(2): 4015044, 1-13.
- Bayrak, O., & Sheikh, S. A. 1998. Confinement reinforcement design considerations for ductile HSC columns. *Journal of Structural Engineering*, 124(9), 999-1010.

- Billah, A. M., and Alam, M. S. 2013. Seismic fragility assessment of high strength reinforced concrete columns considering parameter uncertainty. *ACI Special Publication, SP-293-2*, 1-18.
- Clemena, G.G., and Virmani, Y.P. 2004. Comparing the chloride resistance of reinforcing bars. *Concrete International*, 26(11), 39-49.
- Colaco, J. P. 1985. 75-story Texas Commerce Plaza, Houston-The use of high-strength concrete. *High-Strength Concrete, SP-87*, ACI international, Detroit, MI.
- CSA. 2019. Canadian highway bridge design code. Standard CSA-S6-19, Canadian Standard Association, Rexdale, Ont.
- Cusson, D., and Paultre, P. 1994. High-strength concrete columns confined by rectangular ties. *Journal of Structural Engineering*, 120(3), 783-804.
- D202. 2006. Bridge Standards & Procedures Manual. Volume 3. British Columbia Ministry of Transportation and Infrastructure, Coquitlam, BC.
- Darwin, D., Browning, J., O'Reilly, M., Xing, L., and Ji, J. 2009. Critical chloride corrosion threshold of galvanized reinforcing bars. *ACI Materials Journal*, 106(2), 176-183.
- Elnashai, A. S., and Sarno, L. D. 2008. *Fundamentals of earthquake engineering*, Wiley, New York.
- Elwood, K.J., and Eberhard, M.O. 2009. Effective stiffness of reinforced concrete columns, *ACI Structural Journal*, 106(4), 476-484.
- Ji, J., Darwin, D., and Browning, J. P. 2005. Corrosion resistance of duplex stainless steels and MMFX microcomposite steel for reinforced concrete bridge decks. The University of Kansas Center for Research. INC., Lawrence, KS.
- Kappos, A. J., and Konstantinidis, D. 1999. Statistical analysis of confined high strength concrete. *Materials and Structures*, 32(10), 734-748.
- Konstantinidis, D., and Kappos, A. 2003. Seismic evaluation of R/C buildings using high performance materials. In *Proceedings of Advanced Materials for Construction of Bridges, Buildings, and Other Structures III*, Davos, Switzerland, 7-12 September 2003. Engineering Conferences International, pp. 1-10.
- Laughery, L. 2016. Response of high-strength steel reinforced concrete structures to simulated earthquakes. Ph.D. Dissertation, Purdue University, West Lafayette, IN.
- Légeron, F., and Paultre, P. 2000. Behavior of high-strength concrete columns under cyclic flexure and constant axial load. *ACI Structural Journal*, 97(4), 591-601.
- Li, Y., Cao, S., and Jing, D. 2018. Concrete columns reinforced with high-strength steel subjected to reversed cycle loading. *ACI Structural Journal*, 115(4), 1037-1048.
- Lim, J., Park, H., and Eom, T. 2017. Cyclic load tests of reinforced concrete columns with high-strength bundled bars. *ACI Structural Journal*, 114(1), 197-207.
- Mander, J. B., Priestley, M. J. N., and Park, R. 1988. Theoretical stress strain model for confined concrete. *Journal of Structural Engineering*, 114(8): 1804-1826.
- Menegotto, M., and Pinto, P. E. 1973. Method of analysis for cyclically loaded R.C. plane frames including changes in geometry and nonelastic behavior of elements under combined normal force and bending. *Symposium on the Resistance and Ultimate Deformability of Structures Acted on By Well-Defined Repeated Loads*, International Association for Bridge and Structural Engineering, Zurich, Switzerland, 15-22.
- Moyer, M., and Kowalsky, M. 2003. Influence of tension strain on buckling of reinforcement in concrete columns. *ACI Structural Journal*, 100(1), 75-85.
- Park, R. 1988. Ductility evaluation from laboratory and analytical testing. *Proceedings of the 9th World Conference on Earthquake Engineering*, Tokyo-Kyoto, Japan, Vol. VIII, 605-616.
- Paultre, P., Eid, R., Robles, H. I., and Bouaanani, N. 2009. Seismic performance of circular high-strength concrete columns. *ACI Structural Journal*, 106(4), 395-404.
- Pedro, J. J. O., Reis, A. J., and Baptista, C. 2018. High strength steel S690 in highway bridges. *Stahlbau*, 87(6), 555-564.
- Priestley, M.J.N., Seible, F., and Calvi, G.M. 1996. *Seismic design and retrofit of bridges*. Wiley, New York.
- Rautenberg, J. M., Pujol, S., Tavallali, H., and Lepage, A. 2013. Drift capacity of concrete columns reinforced with high-strength steel. *ACI Structural Journal*, 110(2), 307-317.
- Razvi, S. R., and Saatcioglu, M. 1994. Strength and deformability of confined high-strength concrete columns. *ACI Structural Journal*, 91(6), 678-687.
- Restrepo, J. I., Seible, F., Stephan, B., and Schoettler, M. J. 2006. Seismic testing of bridge columns incorporating high-performance materials. *ACI Structural Journal*, 103(4), 496-504.
- Saleem, M. A., Mirmiran, A., Xia, J., and Mackie, K. 2011. Ultra-high-performance concrete bridge deck reinforced with high-strength steel. *ACI Structural Journal*, 108(5), 601-609.
- SeismoSoft. 2018. SeismoStruct- A computer program for static and dynamic nonlinear analysis of framed structures. Available from URL: www.seismosoft.com
- Seliem, H. M. 2007. Behavior of concrete bridges reinforced with high-performance steel reinforcing bars. Ph.D. Dissertation, North Carolina State University, Raleigh, NC.
- Sritharan, S., Suleiman, M. T., and White, D. J. 2007. Effects of seasonal freezing on bridge Column-Foundation-Soil interaction and their implications. *Earthquake Spectra*, 23(1), 199-222.
- Thomas, A., Davis, B., Dadi, G. B., and Goodrum, P. M. 2013. Case study on the effect of 690 MPa (100 ksi) steel reinforcement on concrete productivity in buildings. *J. Constr. Eng. Manage.*, 139(11): 04013025.
- WJE (Wiss, Janney, Elstner Associates). 2008. Mechanical properties of ASTM A1035 high strength steel bar reinforcement. WJE No. 2008.9901.0. Northbrook, IL: WJE.